NANO · MICRO small

www.small-journal.com

The Role of Liquid Ink Transport in the Direct Placement of Quantum Dot Emitters onto Sub-Micrometer Antennas by Dip-Pen Nanolithography

*Farah Dawood, Jun Wang, Peter A. Schulze, Chris J. Sheehan, Matthew R. Buck, Allison M. Dennis, Somak Majumder, Sachi Krishnamurthy, Matthew Ticknor, Isabelle Staude, Igal Brener, Peter M. Goodwin, Nabil A. Amro, and Jennifer A. Hollingsworth**

Dip-pen nanolithography (DPN) is used to precisely position core/thick-shell ("giant") quantum dots (gQDs; ≥10 nm in diameter) exclusively on top of silicon nanodisk antennas (≈500 nm diameter pillars with a height of ≈200 nm), resulting in periodic arrays of hybrid nanostructures and demonstrating a facile integration strategy toward next-generation quantum light sources. A three-step reading-inking-writing approach is employed, where atomic force microscopy (AFM) images of the pre-patterned substrate topography are used as maps to direct accurate placement of nanocrystals. The DPN "ink" comprises gQDs suspended in a non-aqueous carrier solvent, *o*-dichlorobenzene. Systematic analyses of factors influencing deposition rate for this non-conventional DPN ink are described for flat substrates and used to establish the conditions required to achieve small (sub-500 nm) feature sizes, namely: dwell time, ink-substrate contact angle and ink volume. Finally, it is shown that the rate of solvent transport controls the feature size in which gQDs are found on the substrate, but also that the number and consistency of nanocrystals deposited depends on the stability of the gQD suspension. Overall, the results lay the groundwork for expanded use of nanocrystal liquid inks and DPN for fabrication of multi-component nanostructures that are challenging to create using traditional lithographic techniques.

1. Introduction

Sub-wavelength nanophotonic structures, such as optical nanoantenna and nanoscale resonators, can modify the light emission properties of quantum emitters, including atomic, molecular, and nanocrystalline light emitters. In the latter class of fluorophores, colloidal quantum dots (QDs) have been extensively investigated[1] due to their attributes of size-dependent color tunability (ultraviolet to the mid-infrared), relatively high photoluminescence stability and efficiency, and solution processability. Effects of a photonic structure on QDs and other emitters include enhancement of the radiative rate by the well-known Purcell effect[2] and enhancement of excitation efficiency,[1d] as well as control over the direction[1b,c] and polarization[3,1c] of emitted light. To realize these effects, however, the emitter must be placed in proximity to the nanophotonic structure.

Achieving the necessary control over the placement of an emitter relative to a

Prof. F. Dawood,[+] Dr. J. Wang, P. A. Schulze, C. J. Sheehan, Prof. M. R. Buck,[++] Prof. A. M. Dennis,[+++] Dr. S. Majumder, Dr. S. Krishnamurthy, M. Ticknor, Dr. P. M. Goodwin, Dr. J. A. Hollingsworth
Materials Physics and Applications Division, Center for Integrated Nanotechnologies
Los Alamos National Laboratory
Los Alamos, NM 87545, USA
E-mail: jenn@lanl.gov

The ORCID identification number(s) for the author(s) of this article can be found under https://doi.org/10.1002/smll.201801503.

[+]Present address: Department of Chemistry, Hamilton College, Clinton, NY 13323, USA
[++]Present address: Department of Chemistry, Colgate University, Hamilton, NY 13346, USA
[+++]Present address: Department of Biomedical Engineering and Division of Materials Science and Engineering, Boston University, Boston, MA 02215, USA

Prof. I. Staude
Nonlinear Physics Centre
Research School of Physics and Engineering
The Australian National University
Canberra, Australian Capital Territory 0200, Australia

Dr. I. Brener
Center for Integrated Nanotechnologies
Sandia National Laboratories
Albuquerque, NM 87185, USA

Dr. N. A. Amro
Advanced Creative Solutions Technology
Carlsbad, CA 92008, USA

DOI: 10.1002/smll.201801503

patterned photonic structure for an arbitrary collection of nanoscale optical antenna and a myriad of potential quantum emitters remains a daunting lithographic challenge. The two components of the desired hybrid structure often have different beginnings. Photolithography,[4] electron-beam lithography,[4] focused ion-beam lithography,[5] and nanoimprint lithography[6] are widely used to generate micro- and nanostructured architectures, such as nanoantennas, while colloidal QDs, for example, are prepared using low-temperature, solution-phase synthesis techniques. The integration of patterned "hard" metallic or dielectric structures and "soft" materials, like molecules, polymers, or nanomaterials, remains a significant challenge related both to materials incompatibility, e.g., some soft materials would be damaged by the high energy or high temperature conditions employed for many of the traditional lithographic techniques, and the need to pair such disparate materials with nanoscale registry.

When the nanoantennas or resonators are made of gold, this challenge can be surmounted by chemically functionalizing the gold surface such that nanocrystalline emitters possessing complementary chemical functionalization preferentially adhere to the metal.[1b,d,7] However, there has been increased interest in all-dielectric nanoantennas due to lower losses at optical frequencies and enhanced functionality compared to metallic plasmonic nanoantennas,[8] and these pose new challenges for secondary integration of a quantum emitter. Selective coupling of emitters to such antenna using chemical functionalization strategies requires equally selective functionalization of, for example, silicon nanodisks on a Si or glass substrate.[8b] Compared to the facile functionalization of metallic structures on a Si or glass substrate that takes advantage of the strong affinity of thiol moieties for Au, dielectric antenna is less easily targeted. Instead, multistep processes involving top-down electron-beam lithography have been necessary for the selective functionalization of Si nanodisks and subsequent placement of QDs.[9]

Here, we describe an approach using dip-pen nanolithography (DPN) for the direct placement of QDs onto all-dielectric nanoantennas comprising arrays of 3D Si pillars. DPN is a scanning probe-based alternative lithography technique that uses an atomic force microscopy (AFM) tip to deliver a broad range of "inks" such as small organic molecules, peptides, proteins, polymers, metal ions, and colloidal nanoparticles on a diverse set of surfaces with nanoscale precision.[10] DPN is a mask-free, room-temperature process that does not deleteriously impact the inherent properties of an ink. The majority of previous DPN work, however, has been carried out on flat, featureless substrates. DPN was recently used to deposit molecular inks onto 3D structured substrates, i.e., oligonucleotides inside gold microwells[11] and phospholipids on top of microresonators,[12] but the demonstration of DPN on nanostructured arrays has not yet been achieved.

The most common type of ink used for DPN comprises small molecules that are transported from an AFM tip to a substrate by diffusion through a water meniscus, which forms spontaneously at the tip-substrate interface in a high humidity environment. (The DPN instrument is situated in a humidity-controlled chamber.) Diffusive inks are necessarily water-soluble and their transport is dominated by molecular diffusion processes.[13] These inks are not amenable to direct "writing" of nanoparticles. By contrast, liquid inks exhibit bulk fluid flow from the AFM tip to a substrate. Aqueous liquid inks consist of water-soluble high-molecular-weight materials, such as polymers and dendrimers, that can be used as carriers for other components of an ink, including nanoparticles.[13,14] Comparatively, nonaqueous liquid inks are the least commonly applied inks to date. Such inks form a "capillary bridge" between the AFM tip and substrate that comprises the ink itself, rather than water.[13] Transport models based on Laplace pressure differences and surface capillary forces[15] have been described for the fluid flow of both types of liquid inks. The impact of various DPN experimental parameters on the forces influencing flow rate, including dwell time, surface energy, ink viscosity, and volume of ink on the tip have begun to be explored,[13,14] with reports differing as to which factor—ink viscosity[15a,b] or on-tip volume[15c,d]—has the greatest impact.

In this work, we report the selective deposition of a limited number of thick-shell or "giant" core/shell QD (gQD) emitters on the tops of Si nanoantennas, where these larger QDs were chosen due to their significantly enhanced chemical and photostability compared to conventional QDs.[16] To adequately locate the gQDs onto the tops of these sub-micrometer (≈500 nm) surfaces, we elaborate a three-step "reading–inking–writing" DPN process. Furthermore, to realize the required control over feature size, we investigate a range of DPN parameters influencing absolute deposition rates and rate regularity. Specifically, we quantify the impact of dwell time (tip–substrate contact time), ink–substrate contact angle, and ink volume on the process of liquid ink transport and, thereby, the rate of formation of written features. We further determine conditions for which the nanocrystal ink behaves like a single-component liquid compared to when the carrier solvent and the nanocrystal exhibit partially divergent transport trends. Taken together, our results uniquely elucidate the utility of nonaqueous, nonpolymer, low-volatility solvents (e.g., *o*-dichlorobenzene, *o*-DCB) as carriers to mediate the precision placement of large (≥10 nm) nanocrystals onto complex, 3D nanoscale surfaces.

2. Results and Discussion

2.1. Nanocrystal Liquid Ink and Substrate Characteristics

The key parameters influencing liquid transport have been well elucidated for aqueous liquid inks,[17] as well as for a model nonaqueous liquid ink comprising Nordland optical adhesives (NOAs) of varying viscosity and surface tension.[15c,d] A similar understanding is lacking for nanocrystal liquid inks and is established here for two different sizes of nanocrystals—≈10 nm diameter (diameter: 9.5 ± 0.3 nm) PbS/CdS, CdSe/CdS, or InP/CdSe core/shell gQDs and ≈20 nm CdSe/CdS core/shell gQDs—suspended in low-volatility *o*-DCB (boiling point: 180.5 °C) at a concentration of $\approx 10^{-5}$ M. Differences in QD core composition are not expected to affect the behavior of these QDs as inks, as the shell composition and surface ligand chemistry (principally oleate molecules[18]) are

identical. As described below, however, we do observe an effect of QD diameter (≈10 nm vs ≈20 nm) on the stability of the nanocrystal ink, which impacts the QD transfer process.

The balance of forces between surface tension and ink–substrate interaction energies determines the wettability or angle of contact of the liquid ink on a given substrate, with larger DPN feature sizes the expected result of higher wettability (lower contact angles).[17] Below, we compare spot sizes obtained on two different substrates—hydrophilic (oxygen plasma treated) and hydrophobic (as received) Si. The degree to which we were able to use differences in ink–substrate interaction energies to tune spot size was reduced, however, by our choice of carrier solvent; namely, *o*-DCB is neither extremely polar (2.7 P′ polarity compared to water's 10.2 P′) nor extremely nonpolar (compared to hexane's 0.1 P′). Nevertheless, a substrate effect based on ink–substrate contact angle was observed.

2.2. Extended-Writing Protocol to Assess Nanocrystal Liquid-Ink Transport Properties

Arrays of 5 × 5 spots were written in a raster pattern with a pitch of 4–8 µm (**Figure 1**). From 12 to 22 arrays were written following a single pen-inking step, resulting in from 300 to 550 spots, respectively. Spot diameter as a function of spot number is shown in Figure 1b for a 2 s dwell time on both hydrophilic and hydrophobic substrates (see Figure S1 of the Supporting Information for a shorter 0.01 s dwell time). The observed quasi-exponential decay in spot size is similar to that described for NOA liquid inks subjected to a similarly long writing protocol,[15d] which was attributed to depletion of the ink volume on the AFM tip over time and resulting reduction of the Laplace pressure gradient that is responsible for mass transfer from tip to substrate.[15c,d] In this way, the transfer of ink from tip to substrate that occurs during each step of the writing process directly affects the rate of deposition for a subsequent step for both the simple and the nanocrystal liquid inks, but, significantly, near-constant spot sizes can be realized later in an array cycle.

An additional effect of the dynamic nature of on-tip volume is apparent in the pattern of spot sizes within individual arrays. Namely, the first spots in each array are larger than the remaining spots, resulting from a temporary recovery in on-tip volume that takes place during a one minute interval that separates each array (Figure 1b, inset). During this time, on-tip ink volume can be partially recovered by way of capillary-action-mediated movement of ink located on the upper regions of the cantilever to the writing tip. Thus, ink initially located away from the writing tip can constitute an active "reservoir" of ink that communicates with the tip in response to on-tip volume loss incurred in writing.[15d]

The effect is more apparent for arrays written on the hydrophilic substrate than on the hydrophobic substrate (compare Figure 1b with Figure S2, Supporting Information). Here, we note that the degree to which the QD-*o*-DCB ink wets the different substrates is distinct and likely plays a role in the observed spot-size trends. Specifically, measured contact angles were ≈3°–5° and ≈15°–20° for the hydrophobic and the hydrophilic substrates, respectively. While both ranges encompass small contact angle values, indicating appreciable wetting of the surface in either case, using a spherical cap approximation method[19] to calculate spot volumes from spot diameter and contact angle (see the Experimental Section), we find that spot volumes on the hydrophilic substrate are in fact larger than on the hydrophobic surface, despite larger spot spread on the latter (compare Figure 1b and Figure S1 with Figure S3, Supporting Information). Thus, the dramatic spikes in first-spot size in the case of the hydrophilic substrate can be understood as resulting from greater depletion in on-tip volume following each array deposition, with enhanced depletion causing greater ink flow from the reservoir region. The consequence would be larger differences in on-tip volume between the steps of last and first-spot depositions in consecutive arrays and, thereby, larger differences in last and first spot sizes in these arrays, as is observed.

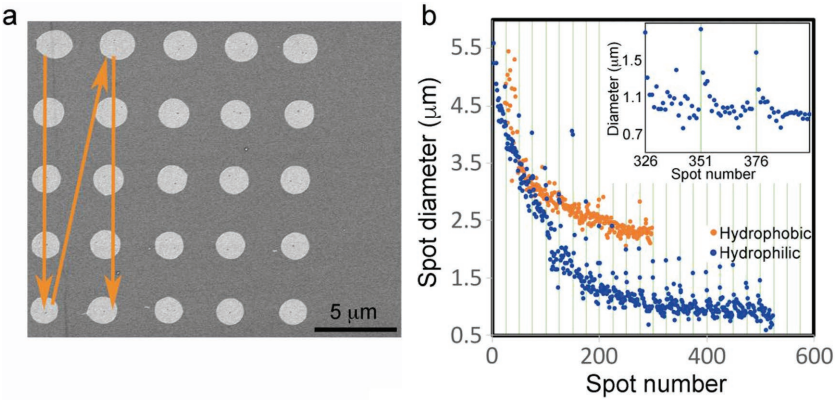

Figure 1. a) Representative scanning electron microscopy (SEM) image showing a 5 × 5 array. The bright contrast is created by the QDs. b) Spot-diameter decay for a long dwell time of 2 s obtained for either a hydrophobic or a hydrophilic substrate. Inset: spot-size spiking in first spots of each array for spots on the hydrophilic substrate; vertical lines indicate the position of the first spot in each array.

2.3. Understanding the Transitions from Dynamic to Steady-State Writing Regimes

Transforming spot diameter trends into spot volume trends using calculated volumes (Figure S3, Supporting Information), we determine the average volume deposited per array and show that it decreases with array number as ink is depleted from the cantilever and the deposition rate is progressively reduced (**Figure 2**a). Substrate-dependent differences in deposition rate are very apparent in early arrays (even if the contact angle for the hydrophilic substrate is assumed to be <17° and that for the hydrophobic substrate >3°–horizontal markers in Figure 2a), but diminish in later arrays (Figure 2a), such that only dwell time differentiates writing protocol at late arrays (Figure 2a, inset: arrays 9 and 10). A plot of average array volume as a function of total deposited ink (Figure 2b)

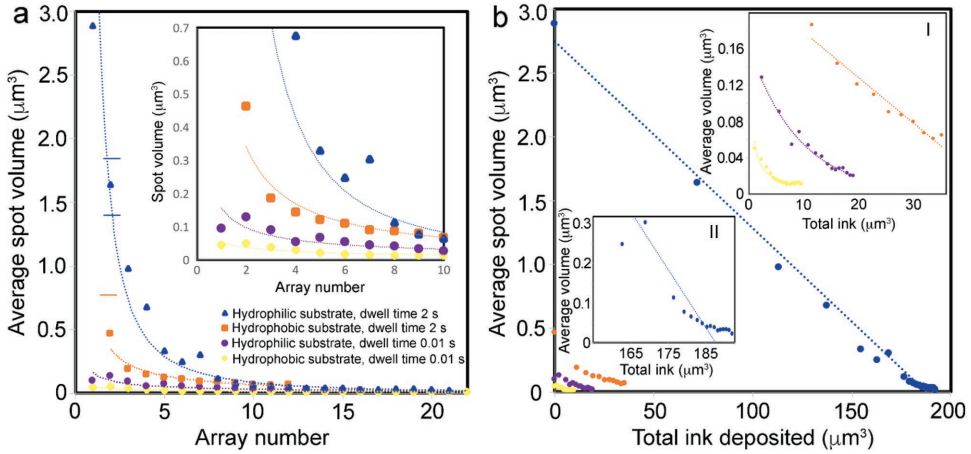

Figure 2. a) Average spot volume in an array as a function of array number for different surfaces (17° and 3° contact angles used for volume calculations for hydrophilic and hydrophobic substrates, respectively) and dwell times. Each decay can be fit to a simple power law function (blue triangle: $R^2 = 0.96$, $k = -1.8$; orange square: $R^2 = 0.94$, $k = -1.0$; purple circle: $R^2 = 0.88$, $k = -0.7$; yellow diamond: $R^2 = 0.88$, $k = -0.6$). Blue horizontal lines represent volume assuming 15° (bottom) and 19° (top) contact angles; orange horizontal line represents volume assuming 5° contact angle. b) Average spot volume in an array as a function of calculated total deposited ink. Trajectories for spots written on hydrophilic substrates can be fit with a line; however, closer inspection of later-array trends reveals strong deviation from a simple linear relationship. (Writing protocol are as indicated in (a)). Inset I: close-up for a 2 s dwell time and hydrophobic substrate, as well as a 0.01 s dwell time for each substrate. Inset II: close-up of later-array region for a 2 s dwell time and hydrophilic substrate.

makes evident the striking difference in total volume deposited at the long dwell time (2 s) on a hydrophilic substrate compared to any other combination of dwell time and substrate. Our data suggest a linear decay can be applied to spots deposited for 2 s dwell times, while power law and exponential decays provide the best fits for the 0.01 s dwell time series on hydrophilic and hydrophobic substrates, respectively (Figure 2b, inset I). That said, we hesitate to ascribe physical significance to these simple mathematical fits.

Instead, we suggest that the trajectories might be best described as comprising two distinct regimes. In the first regime the volume of ink on the cantilever is changing rapidly but there is sufficient ink on the cantilever to provide quick replacement of ink that is lost through deposition, keeping the deposition rate high and yielding the majority of deposited ink (≈85%).

In the second regime, by contrast, average spot size is relatively more constant, suggesting a more constant on-tip volume that is likely in equilibrium with the remaining reservoir volume.

In other words, in regime one, we suggest there is a continuous flow of ink from reservoir to tip during writing as opposed to in response to writing, as in regime two. Indeed, the trajectory for the 2 s dwell time on the hydrophilic surface can be separated into two such regimes. The simple linear regime only holds for the first 5–10 arrays in which the majority of ink is deposited, while relatively little ink is deposited in the remaining arrays possessing approximately constant-size spots (Figure 2b, inset II).

The long 2 s dwell time yields larger spot volumes compared to the ultrashort 0.01 s dwell time, as is expected, and this is the case whether considering spots at the beginning or the end of an array series. However, the differences in spot volumes are not proportional to the ratio of the dwell times. While dwell times differ by a factor of 200, early-array average spot volumes for both substrates differ by only ≈10–15 times, and steady-state average spot volumes differ by only ≈5 and ≈2.5 times on the hydrophobic and the hydrophilic substrates, respectively (Figure 2a, inset). Thus, dwell time plays a greater role early in a long writing cycle compared to its effect once the steady-state regime has been reached, but in neither regime do volume trends follow linearly with changes in dwell time.

Ink–substrate interactions strongly influence volume deposition. The total volume deposited on the hydrophilic substrate is >4 times that deposited on the hydrophobic substrate for the same long dwell time of 2 s, for example (Figure 2b). Thus, if the goal of a writing procedure is to control spot-size spread (spot diameter), e.g., when needing to target a small area, then higher contact angles are necessary. By contrast, if it is more important to limit spot volume, e.g., when using the liquid as a carrier for nanocrystals where the number of deposited particles should be proportional to spot volume (and a function of nanocrystal concentration) rather than simply spot diameter, then a high ink–substrate wettability would be advantageous.

2.4. Number of Printed QDs Qualitatively Follows Spot-Volume Trend But with Substrate Effects Overlaid

The number of QDs deposited per spot is initially high then decays in a manner similar to that observed for spot volume decay (**Figure 3**). The further observation that larger numbers of dots are deposited per spot written on hydrophilic substrates agrees with the larger spot volumes calculated for these surfaces; however, the relative differences appear exaggerated when comparing similar-volume spots for the same long 2 s dwell time on the two substrates. For example, a 0.65 μm² spot written on the hydrophilic substrate yielded 360 QDs (spot #128), while a 0.60 μm² spot written on the hydrophobic substrate yielded ≈110 QDs (spot #28). Similarly, a 0.14 μm²

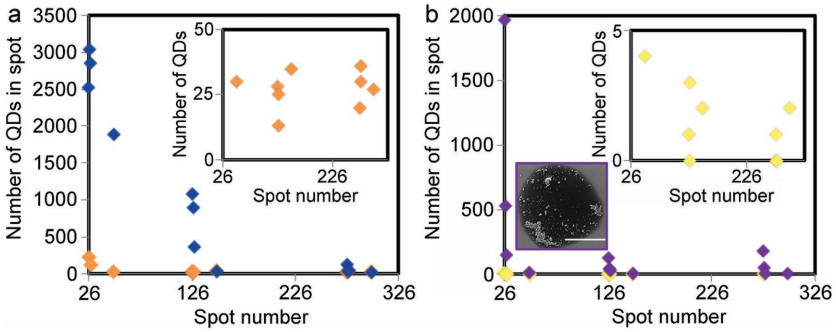

Figure 3. Measuring the number of QDs printed per spot over time for different writing protocol: a) 2 s dwell time on hydrophilic (blue) and hydrophobic (orange) substrate, b) 0.01 s dwell time on hydrophilic (purple) and hydrophobic (yellow) substrate. SEM image shows spot 27 on the hydrophilic substrate (scale bar = 1 μm).

spot on the hydrophilic substrate yielded 280 QDs (spot #150), while a 0.11 μm^2 spots on the hydrophobic substrate yielded only 35 (spot #150) QDs. While it is possible that our contact angle calculations underestimated and overestimated volumes for the hydrophilic and hydrophobic substrates respectively, other factors including droplet shape (domed vs flat, respectively) and direct QD-substrate adhesive or repulsive forces may influence QD deposition rate.

Comparing QD deposition for spots written on identical substrates, thereby eliminating possible discrepancies in spot-volume determinations, we find that more QDs are deposited in similar-volume spots if the spot is located in an early-array position compared to a later point in the writing protocol. Namely, on the hydrophilic substrate, calculated spot volumes of 0.15 μm^3 yielded ≈150 QDs for spot #28 deposited using a 0.01 s dwell time and ≈30 QDs for spot #150 deposited at a 2 s dwell time. (Note: these spots were chosen to avoid the first-spot spiking effects.) As discussed above, liquid deposition rate is fastest earlier in the array cycle. This faster flow of liquid from tip to substrate appears to cause a greater transfer of QDs for a given volume of carrier liquid ink. We observe that whether many or a few QDs are being deposited from a given solvent droplet, with few exceptions the liquid spot defines the region where the QDs are located (from close-packed monolayers of QDs as evident in Figure 1 to sparsely populated spots as shown in Figure 3b: dark region delineates solvent and surfactant residue; bright spots correspond to individual QDs), supporting its role as nanocrystal carrier.

2.5. Optimizing Protocol Timing and Ink Stability Reduces Early-to-Late Array Effects

The dynamic nature of the on-tip volume and the strong influence of tip volume on liquid-ink deposition rate challenge efforts to realize consistent and reproducible feature sizes over time. We find that a simple modification to the writing protocol, such as introducing a 60 s interval between columns within arrays, allows the tip to be recharged with ink from the upper regions of the cantilever, resulting in more consistent feature sizes. The precise duration of this delay period likely depends on the protocol dwell time. 60 s was found adequate to arrest the exponential decay in spot size for a 0.01 s dwell time. The observed tendency for fewer QDs to be deposited in late array compared to early array spots for same-volume features is an additional source of irregularity that impedes efforts toward controlled and predictable writing. We note here that the gQD suspension in *o*-DCB is stable to precipitation but exhibits slight turbidity, implying that the nanocrystals have some tendency to self-associate.[18] This is, in part, an effect of QD size. We find that optically clear suspensions can be prepared by replacing the large-diameter gQDs used to assess deposition as a function of spot number as shown in Figure 3 (diameter: 19.6 ± 2.7 nm) with smaller nanocrystals (diameter: 9.5 ± 0.3 nm). In this case, QD numbers are maintained at high levels in extended writing, as shown in Figure S4 (green symbols) of the Supporting Information.

2.6. Controlling Ink Volume on the Cantilever Tip From Inception: Ink Loading Protocol

As the volume of ink on the cantilever tip is the key variable in controlling deposition rate, to quickly establish a regime of steady-state spot size and, ideally, to minimize spot size, a method is needed to limit the quantity of ink that is on both the cantilever tip and in the upper regions of the cantilever, where the latter serves as an ink reservoir as described above. Briefly, we identified three potential approaches for achieving this result: (a) limiting the time allowed for ink loading (see Figure S5, Supporting Information), (b) excessive "bleeding" of cantilever prior to executing a writing protocol (**Figure 4**), and (c) alternate method for initial delivery of ink to the cantilever (**Figure 5**).

Prior to executing an extended writing protocol, it is necessary to "bleed" the cantilever of extreme excesses of ink. This entails allowing the tip to touch down on the substrate 2–3 times for ≈2 s before the first array spot is written. Here, the resulting bleed regions consisted of large-area depositions, typically ≈5–10 μm in diameter but occasionally up to 40 μm (Figure S6, Supporting Information). The need for an initial tip bleed following ink loading has been reported previously,[20] but uniquely we observe that for a complex ink like the QD/*o*-DCB mixture, the stability of the ink suspension influences the bleed regime. Namely, for the more stable suspensions comprising smaller gQDs (≈10 nm diameter), initial bleed spots are dominated by the carrier solvent. The opposite is the case for less stable inks comprising larger gQDs (≈20 nm diameter; Figure S6, Supporting Information), where the nanocrystals are more prevalent in earlier bleed spots. These observations suggest that less stable inks afford rapid expulsion of QDs from the AFM tip (see Supporting Information).

Even with inclusion of a bleeding step, it is clear that the volume of ink on the cantilever continues to play a significant role in determining spot size. The rapid changes in spot size observed for early-array spots (Figure 2 and ref. [15d]) is

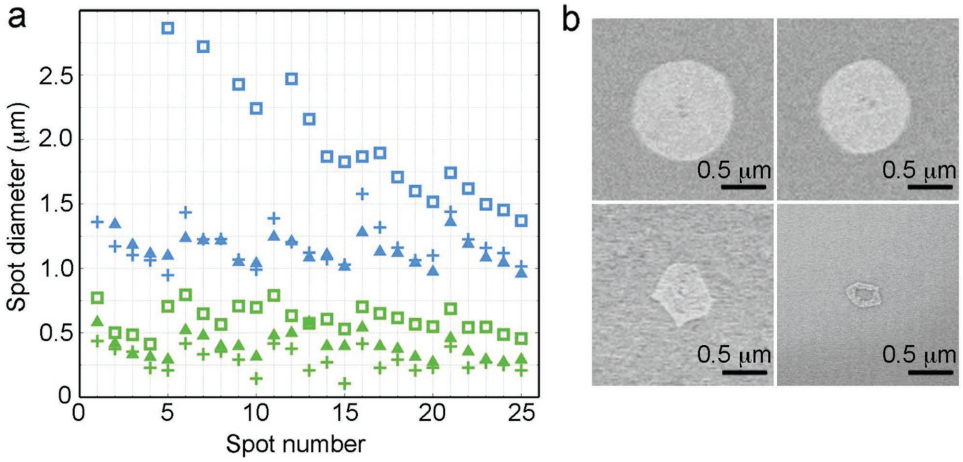

Figure 4. Effect of bleed number on early and late spot sizes in long-term writing protocol. a) Blue: spots written after 9 bleeds for array 1 (square), array 3 (triangle), and array 5 (plus). Green: spots written after 60 bleeds for array 1 (square), array 3 (triangle) and array 5 (plus). b) Top: SEM images of spots written after 9 bleeds in center and at end of array 5, respectively. Bottom: SEM images of spots written after 60 bleeds in center and at end of array 5, respectively. In all images, QDs afford brightest contrast.

a signature of the effective continuation of a bleeding process, albeit in a less dramatic fashion. For this reason, we conducted writing protocol following deposition of different numbers of bleed spots, resulting in different amounts of ink on the cantilever at the start of array writing. Doing so, it was possible both to obtain smaller initial spots and to avoid the regime of volume-dependent deposition rate decay, reaching the quasi steady-state regime early in the array cycle (Figure 4). By combining this approach with a short dwell time (0.01 s), in fact, very small sub-micrometer spots could be written. Averages for arrays 1, 3 and 5 for 5 × 5 array series written after 9 and 60 bleeds were 1936 ± 105, 1138 ± 22, and 1183 ± 32 nm, versus 608 ± 21, 397 ± 19, and 290 ± 18 nm. Both series show within-array, first-column size spiking as a result of the newly applied writing protocol whereby a 60 s pause is allowed between columns in addition to between arrays. Lastly, while the spots in array 5 following the excessive bleeding protocol do indeed fall well below 1 μm in size, even below diameters of only 250 nm (Figure 4a), which is desirable for writing on small structures, the spots created in this very low on-tip volume regime become irregularly shaped and lack ink in the spot centers (Figure 4b).

Finally, in several reports, a fundamentally different approach than dip-coating has been employed as an inking method. The method entails raster-scan coating the tip through a partially evaporated microdroplet of ink, which leaves the underside and upper regions of the cantilever free of ink, eliminating the need for tip bleeding and reducing the "reservoir effect," as well as some of the dynamic processes leading to spot-size spiking for early-array spots and deposition rate (spot size) decay (Figures 1 and 2).[21] Even though the volume of ink that is subject to coating is small, the scanning motion of this inking method allows the AFM tip to be evenly coated while preventing damage to the tip. For example, in Figure 5 we show the first spots in initial arrays deposited immediately following raster-scan inking of a tip using long (2, 2.5, and 3 s dwell times). Even without a bleeding step, the spots obtained for a first array and a 2 s dwell time approximately the same size as the steady-state spot size obtained for a dip-coated tip and 2 s dwell time after spot number 300 (≈825 nm and ≈1 μm, respectively), and the spot size does not change appreciably for up to 36 spots. Despite the obvious advantages in both controlling on-tip volume and eliminating the large reservoir of ink on

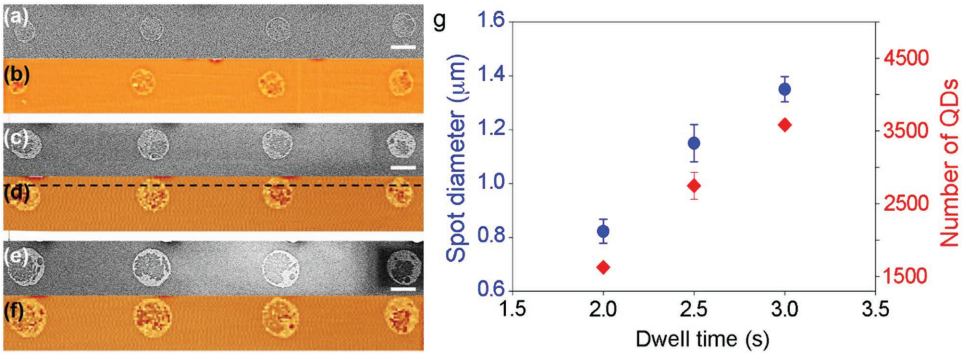

Figure 5. Deposition of InP/CdSe/CdS QD/*o*-DCB ink on Si substrate using the scan-coating method. a,c,e) SEM images of gQDs deposited for 3, 2.5, and 2 s respectively. b,d,f) Corresponding AFM images of (a), (c), and (e). Scale bar represents 1 μm. g) Average QD spot size and number of QDs as a function of dwell time.

the cantilever, raster scanning is more challenging to execute compared to the dip-coating method (requiring precise timing of the raster-scan step with an appropriate degree of solvent evaporation, where the latter is determined by observing an image of the droplet in the optical microscope that is attached to the DPN tool) and may not afford adequate ink loading for extended-writing protocol.

2.7. Applying New Understanding of Liquid-Ink Transport to Delivery of QDs to Sub- Micrometer Optical Antenna

A three-step reading-inking-writing process was elaborated for the controlled deposition of gQDs onto sub-micrometer Si nanodisk arrays (**Scheme 1**). First, substrate topography is "read" by obtaining an AFM image of the Si array using a lower spring constant A-type AFM probe (0.1 N m^{-1}) or with the same higher spring constant M-type AFM probe that is used for writing (2.6 N m^{-1}) (Scheme 1, Step 1; see Supporting Information for detailed descriptions of the two variations of the three-step procedure). The resulting AFM image affords a 3D map of the nanostructured surface at a resolution below the optical diffraction limit of the built-in DPN microscope that is used to guide subsequent writing steps.[21a] Second, an M-type AFM probe is loaded with ink using either the scan-coating or the dip-coating method. Finally, the "writing" step is performed by moving an inked AFM tip to the desired position on the substrate as guided by the previously obtained AFM image (Scheme 1, Step 3; see Supporting Information for expanded experimental description).

Images of Si pillars after QD deposition by variations of the three-step writing process are shown in **Figure 6**. Use of a scan-coated tip yielded approximately uniform QD clusters on the tops of 16 pillars, without unwanted deposition onto areas surrounding the pillars (representative pillars shown in Figure 6a–d). The QDs in this case do not form simple monolayers but, instead, clump together in multilayer piles, perhaps resulting from the quasi-dry condition of the QD-*o*-DCB ink that can result from the scan-coating process. Nevertheless, each pillar received QDs and coverage area is similar for each (Figure S7, Supporting Information).

By contrast, the QDs deposited from a dip-coated tip form monolayer depositions indicative of the carrier solvent dominating the tip-to-surface transfer process as demonstrated above on flat substrates, such that slow evaporation of the *o*-DCB after deposition allows the nanocrystals to self-assemble into roughly close-packed monolayers (Figure 6e–h). Also as observed for flat substrates, controlled writing with dip-coated tips on the nanoantennas requires reducing the ink volume on the cantilever through either extensive writing and/or extensive tip-bleeding. Therefore, a large 5 × 10 array was executed, where Si pillars constituted the target locations. Initial spots were large and QDs overflowed the pillars, but pillars located later in the array could be exclusively targeted with the QDs (Figure 6e–h). Interestingly, the largest spots yielded no QDs on the pillar, suggesting that with sufficiently large spot volumes, the pillar does not effectively hold the liquid as it flows directly to the surrounding substrate. As shown in Figure 6i, in the latter half of the 50-pillar array, a substantial number of pillars had QDs deposited exclusively on them rather than also on the surrounding substrate floor (indicated as "1" rather than "0" in the figure; an example of a gQD-coated pillar designated as "0" is shown in the inset). This extended deposition was conducted following 40 bleeds and using a dwell time of 1 s. By increasing the number of bleeds to 170 and decreasing dwell time to 0.05 s, we were able to improve the uniformity of depositions. In this case, DPN was performed on optically transparent substrates such that gQD photoluminescence could be imaged and quantified (Figure 6j,k), demonstrating both that the emitter retains its ability to photoluminescence following the DPN procedure and that per-pillar intensity is approximately constant, especially for rows 3–5. Overall, it is evident that with adequate control over tip/cantilever volume the dip-coating method likely represents a more technologically relevant process, as larger antenna arrays can be addressed.

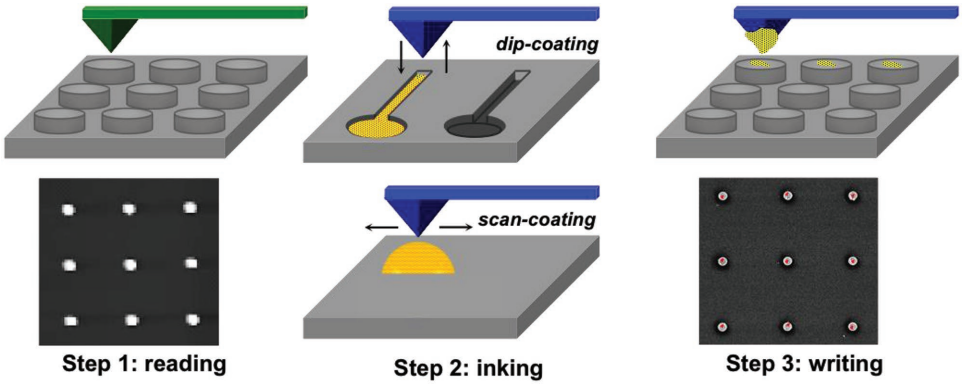

Scheme 1. Three-step "reading–inking–writing" process for depositing ink on a nanostructured surface. (Step 1) Reading is performed by scanning an AFM tip over the surface of the nanodisk array. The resulting AFM image is stored in the instrument software. (Step 2) The AFM tip is inked with the gQD ink using either of two methods: "dip-coating" (top) and "scan-coating" (bottom) in preparation for deposition. (Step 3) The gQD liquid ink is written onto the nanodisks, where the inked AFM tip from Step 2 is brought into contact with the substrate. Demonstrated variations for the approach entail using two different tips for Steps 1 and 2/3 (including a manual method for realigning after the tip is changed from an A-type for reading and an M-type for inking/writing) or using the same tip for all steps, which includes a fast rescan in the vicinity of the target area following inking (see Supporting Information for details).

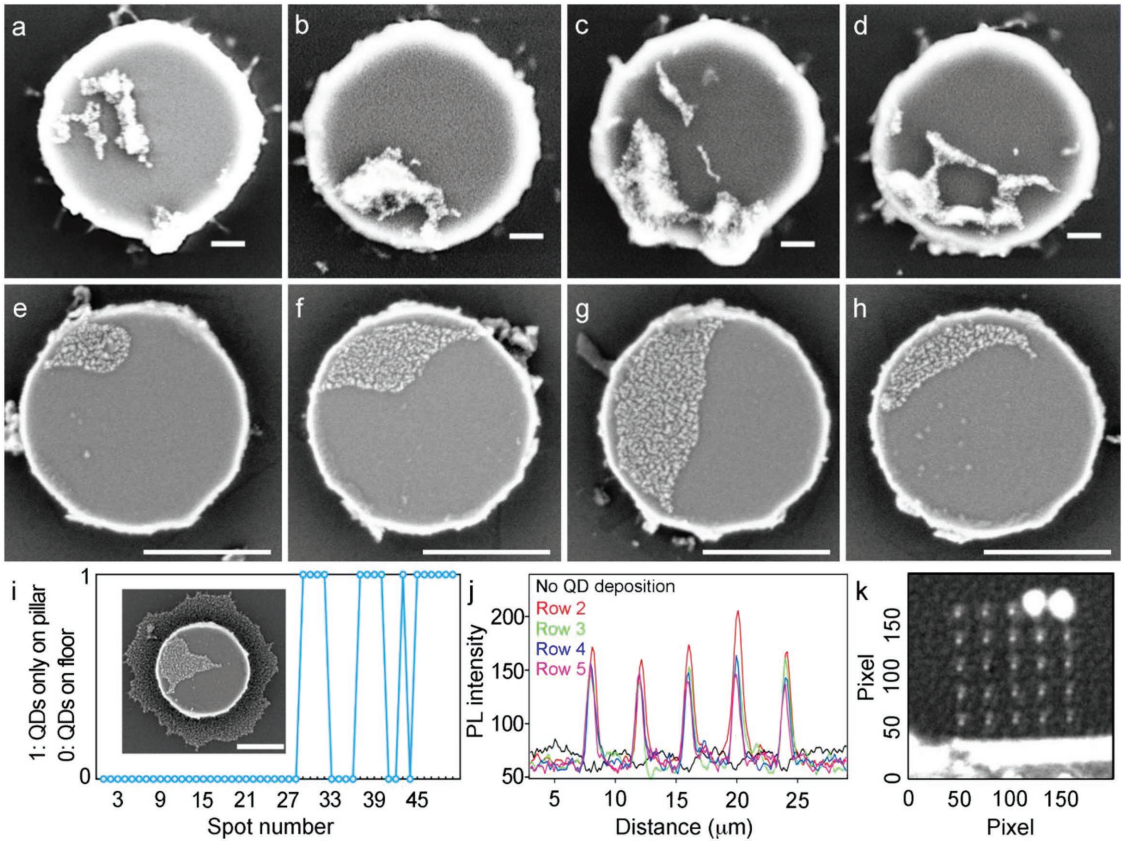

Figure 6. DPN placement of QDs onto silicon nanodisk arrays. a–d) SEM images of InP-5CdSe-3CdS gQDs deposited from a scan-coated tip (2 s dwell time; scale bars are 100 nm). Four of sixteen pillars are shown with depositions representing early, middle, and late writing, respectively. e–h) PbS/CdS gQDs deposited from a dip-coated tip (scale bars are 400 nm). 4 of 50 pillars are shown representing the second half of the writing protocol. i) "Targeting success" for dip-coated tips binned as either QDs present on the substrate around a pillar (rank "0"; inset shows example; scale: 350 nm) or QDs found exclusively on pillar (rank "1"). j) Photoluminescence intensity obtained for pillars decorated with gQDs extracted from k) optical images. Rows are numbered 1–5 from top to bottom of the image shown in (k).

3. Conclusions

Compared to molecular inks, liquid inks have received less attention as agents for the direct writing of nanoscale features by DPN or other scanning probe techniques. Furthermore, comprehensive analyses of the parameters responsible for bulk fluid transfer of liquid inks from an AFM tip to a substrate have been limited to simple nonaqueous liquids[15c,d] or polymer or polymer-containing inks.[15a,b] Here, we provided a detailed examination of the factors governing DPN of complex nonaqueous liquid inks comprising a carrier solvent and suspended nanocrystals without assistance from a polymer matrix. The large size of the nanocrystals (≈10–20 nm gQDs) and the nonpolar nature and low-volatility of the chosen carrier solvent (*o*-DCB) necessitated that ink transfer involve solvent-mediated liquid transport. This is in contrast not only with conventional molecular ink transport that makes use of a spontaneous water meniscus formed in the high-humidity DPN chamber, but also with inks comprising ultrasmall, charged nanocrystals (≤5 nm) deposited from "dry" inks that, like molecular inks, can take advantage of a water bridge between tip and substrate.[22]

Overall, while ink–surface interactions (contact angle) and dwell time could be used to tune spot size, volume effects were found to dominate deposition rates and, thereby, spot diameter and volume, with the solvent "footprint" defining the location of deposited QDs. Both the ink volume immediately available on the writing tip and the volume of "reservoir" ink on the regions of cantilever above the tip strongly influenced the initially achievable spot sizes as well as the consistency of spot size over time. Importantly, adequate control over on-tip volume could be achieved by employing the raster-scan coating method for ink loading, as used previously for some nanocrystal inks,[21] but the total number of features that can be written and the liquid nature of the ink may be compromised in this case. Alternatively, we showed that a simpler dip-coating method could be employed but that it had to be paired with a method for depleting excess ink volume, for example, extreme tip-bleeding. Doing so afforded rapid access to an approximately steady-state deposition rate for writing numerous similarly sized spots. Finally, we demonstrated a three-step reading–inking–writing method for directly coupling nanocrystal quantum emitters, like the large (≥10 nm in diameter) and extremely photostable gQDs shown here, and 3D structured nanoantenna substrates. In this way, DPN is a viable tool for creating new functional multicomponent systems and devices integrated at the nanoscale.

4. Experimental Section

Preparation of gQD Inks: InP/CdSe/CdS, PbS/CdS, and CdSe/CdS gQDs were synthesized according to refs. [16b,18] and/or ref. [23]. After isolation via centrifugation, the gQDs were resuspended in *o*-dichlorobenzene (Sigma-Aldrich) for a final ink concentration of ≈(0.5–1.5) × 10^{-5} M.

Three-Step Deposition Process Using DPN: gQD deposition was carried out using a DPN 5000 system (NanoInk, Skokie IL). Unless otherwise noted, deposition was performed at 25 °C and ≈40–55% relative humidity (RH). Detailed experimental procedures are available in the Supporting Information, where two distinct three-step processes are described—one that entails using an A-type tip for imaging and an M-type tip for writing and another that uses the same M-type tip for both processes.

Contact Angle Measurements: Contact angle measurements were carried out using the sessile-drop methods on a contact angle goniometer (CAMPLUS). 5 µL of each ink was placed on the silicon or nanodisk substrates and measurements were carried out after 60 s. It is noted that the 3°–5° value obtained for the *o*-DCB ink on the hydrophobic substrate is discernible from the situation of complete wetting, e.g., wetting by *o*-DCB is visibly less compared to a very nonpolar solvent, octane.

Scanning Electron Microscopy, Energy Dispersive X-Ray Spectroscopy, and Atomic Force Microscopy for Characterization: Scanning electron microscopy (SEM) images were collected using an FEI Magellan 400. Specific imaging conditions are as follows: concentric backscatter detector, 6 kV beam energy, 4 kV stage bias thus 2 kV landing energy, 0.2 nA beam current, immersion lens mode. SEM data collection did not require coating the samples with a conductive metal. Energy dispersive X-ray spectroscopy and elemental mapping images were acquired using an EDAX Apollo XP-SDD (silicon drift detector). High-resolution AFM imaging for analysis of extended array writing was performed using a Veeco Enviroscope (Model: Escope) with controller model Nanoscope IVA.

Calculating Droplet Volume Using the Spherical Cap Approximation Method: The spherical cap method[19] was used to calculate spot volumes in the extended writing experiments. Here, the spot base is assumed to be circular and the contact angle constant around its base. Volumes of deposited liquid droplets, which upon evaporation afford the observed spots, were calculated according to

$$V = \frac{\pi D^3}{24}\left(\frac{2-3\cos\theta+\cos^3\theta}{\sin^3\theta}\right) \quad (1)$$

where D is the diameter of the measured spot and θ is the measured liquid–substrate contact angle in radians, such that, due to the contribution to droplet volume from the contact-angle-dependent droplet height, larger spot diameters can afford smaller droplet volumes as their heights are lesser compared to droplets formed for larger contact angles (compare Figure 1b with Figure S2, Supporting Information).[19]

Supporting Information

Supporting Information is available from the Wiley Online Library or from the author.

Acknowledgements

F.D. and J.W. contributed equally to this work. F.D. was supported by postdoctoral funding of the Center for Integrated Nanotechnologies (CINT), an Office of Science (OS) Nanoscale Science Research Center (NSRC) and User Facility operated for the U.S. Department of Energy (DOE) by Los Alamos National Laboratory (LANL; Contract No. DE-AC52-06NA25396) and Sandia National Laboratories (Contract No. DE-NA-0003525), and the work was performed in large part at CINT and contributed to CINT User Project, C2013B0048. J.W., P.A.S., S.M., M.T., and J.A.H. acknowledge LANL Directed Research and Development Funds. C.J.S. is a CINT-funded technical specialist. M.R.B. was funded by an LANL Director's Postdoctoral Fellowship, and A.M.D. by a Single Investigator Small Group Research Grant (2009LANL1096), Division of Materials Science and Engineering (MSE), Office of Basic Energy Sciences (OBES), OS, DOE. Los Alamos National Laboratory, an affirmative action equal opportunity employer, is operated by Los Alamos National Security, LLC, for the National Nuclear Security Administration of the DOE under Contract No. DE-AC52-06NA25396.

Conflict of Interest

The authors declare no conflict of interest.

Keywords

dip-pen nanolithography, nanofabrication, optical nanoantenna, quantum dots

Received: April 19, 2018
Revised: May 14, 2018
Published online: June 27, 2018

[1] a) K. Tanaka, E. Plum, J. Y. Ou, T. Uchino, N. I. Zheludev, *Phys. Rev. Lett.* **2010**, *105*, 227403; b) A. G. Curto, G. Volpe, T. H. Taminiau, M. P. Kreuzer, R. Quidant, N. F. van Hulst, *Science* **2010**, *329*, 930; c) G. Rui, W. Chen, D. C. Abeysinghe, R. L. Nelson, Q. Zhan, *Opt. Express* **2012**, *20*, 19297; d) E. Bermúdez Urena, M. P. Kreuzer, S. Itzhakov, H. Rigneault, R. Quidant, D. Oron, J. Wenger, *Adv. Mater.* **2012**, *24*, OP314; e) F. Wang, N. S. Karan, H. M. Nguyen, Y. Ghosh, C. J. Sheehan, J. A. Hollingsworth, H. Htoon, *Nanoscale* **2015**, *7*, 9387; f) K. Matsuzaki, S. Vassant, H.-W. Liu, A. Dutschke, B. Hoffmann, X. Chen, S. Christiansen, M. R. Buck, J. A. Hollingsworth, S. Götzinger, V. Sandoghdar, *Sci. Rep.* **2017**, *7*, 42307.
[2] E. M. Purcell, *Phys. Rev.* **1946**, *69*, 37.
[3] T. H. Taminiau, F. D. Stefani, F. B. Segerink, N. F. van Hulst, *Nat. Photonics* **2008**, *2*, 234.
[4] A. del Campo, E. Arzt, *Chem. Rev.* **2008**, *108*, 911.
[5] A. Tseng, *Small* **2005**, *1*, 924.
[6] S. Y. Chou, *MRS Bull.* **2001**, *26*, 512.
[7] J. Abramson, M. Palma, S. J. Wind, J. Hone, *Adv. Mater.* **2012**, *24*, 2207.
[8] a) A. E. Krasnok, A. E. Miroshnichenko, P. A. Belov, Y. S. Kivshar, *Opt. Exp.* **2012**, *20*, 20599; b) I. Staude, A. E. Miroshnichenko, M. Decker, N. T. Fofang, S. Liu, E. Gonzales, J. Dominguez, T. S. Luk, D. N. Neshev, I. Brener, Y. S. Kivshar, *ACS Nano* **2013**, *7*, 7824; c) J. Cambiasso, G. Grinblat, Y. Li, A. Rakovich, E. Cortés, S. A. Maier*Nano Lett.* **2017**, *17*, 1219; d) M. Caldarola, P. Albella, E Cortés, M Rahmani, T. Roschuk, G. Grinblat, R. F. Oulton, A. V. Bragas, S. A. Maier, *Nat. Commun.* **2015**, *6*, 7915.
[9] I. Staude, V. K. A. Sreenivasan, I. Shishkin, K. Samusev, M. Decker, D. N. Neshev, A. V. Zvyagin, Y. S. Kivshar, *Phys. Status Solidi RRL* **2014**, *8*, 710.
[10] a) D. S. Ginger, H. Zhang, C. A. Mirkin, *Angew. Chem., Int. Ed.* **2004**, *43*, 30; b) K. Salaita, Y. Wang, C. A. Mirkin, *Nat. Nanotechnol.* **2007**, *2*, 145.
[11] R. J. Stokes, J. A. Dougan, D. Graham, *Chem. Commun.* **2008**, 5734.

[12] a) U. Bog, T. Laue, T. Grossmann, T. Beck, T. Wienhold, B. Richter, M. Hirtz, H. Fuchs, H. Kalt, T. Mappes, *Lab Chip* **2013**, *13*, 2701; b) P. Rath, M. Hirtz, G. Lewes-Malandrakis, D. Brink, C. Nebel, W H. P. Pernice, *Adv. Opt. Mater.* **2015**, *3*, 328.
[13] K. A. Brown, D. J. Eichelsdoerfer, X. Liao, S. He, C. A. Mirkin, *Front. Phys.* **2014**, *9*, 385.
[14] L. Huang, A. B. Braunschweig, W. Shim, L. Qin, J. K. Lim, S. J. Hurst, F. Huo, C. Xue, J.-W. Jang, C. A. Mirkin, *Small* **2010**, *6*, 1077.
[15] a) J. R. Felts, S. Somnath, R. H. Ewoldt, W. P. King, *Nanotechnology* **2012**, *23*, 215301; b) G. Liu, Y. Zhou, R. S. Banga, R. Boya, K. A. Brown, A. J. Chipre, S. T. Nguyen, C. A. Mirkin, *Chem. Sci.* **2013**, *4*, 2093; c) C. D. O'Connell, M. J. Higgins, D. Marusic, S. E. Moulton, G. G. Wallace, *Langmuir* **2014**, *30*, 2712; d) C. D. O'Connell, M. J. Higgins, R. P. Sullivan, S. E. Moulton, G. G. Wallace, *Small* **2014**, *10*, 3717.
[16] a) Y. Chen, J. Vela, H. Htoon, J. L. Casson, D. J. Werder, D. A. Bussian, V. I. Klimov, J. A. Hollingsworth, *J. Am. Chem. Soc.* **2008**, *130*, 5026; b) A. M. Dennis, B. D. Mangum, A. Piryatinski, Y.-S. Park, D. C. Hannah, J. L. Casson, D. J. Williams, R. D. Schaller, H. Htoon, J. A. Hollingsworth, *Nano Lett.* **2012**, *12*, 5545.
[17] D. J. Eichelsdoerfer, K. A. Brown, C. A. Mirkin, *Soft Matter* **2014**, *10*, 5603.
[18] Y. Ghosh, B. D. Mangum, J. L. Casson, W. D. J. Williams, H. Htoon, J. A. Hollingsworth, *J. Am. Chem. Soc.* **2012**, *134*, 9634.
[19] A. I. El Sherbini, A. M. Jacobi, *J. Colloid Interface Sci.* **2004**, *273*, 566.
[20] a) H. Wang, O. A. Nafday, J. R. Haaheim, E. Tevaarwerk, N. A. Amro, R. G. Sanedrin, C. Chang, F. Ren, S. J. Pearton, *Appl. Phys. Lett.* **2008**, *93*, 143105; b) S. Hung, O. A. Nafday, J. R. Haaheim, F. Ren, G. C. Chi, S. J. Pearton, *J. Phys. Chem. C* **2010**, *114*, 9672; c) C. D. O'Connell, M. J. Higgins, R. P. Sullivan, S. S. Jamali, S. E. Moulton, G. G. Wallace, *Nanotechnology* **2013**, *24*, 505301; d) C. D. O'Connell, M. J. Higgins, H. Nakashima, S. E. Moulton, G. G. Wallace, *Langmuir* **2012**, *28*, 9953.
[21] a) E. Bellido, I. Ojea-Jimenez, A. Ghirri, C. Alvino, A. Candini, V. Puntes, M. Affronte, N. Domingo, D. Ruiz-Molina, *Langmuir* **2012**, *28*, 12400; b) B. Li, C. F. Goh, X. Zhou, G. Lu, H. Tantang, Y. Chen, C. Xue, F. Y. C. Boey, H. Zhang, *Adv. Mater.* **2008**, *20*, 4873.
[22] W. M. Wang, R. M. Stoltenberg, S. Liu, Z. Bao, *ACS Nano* **2008**, *2*, 2135.
[23] C. J. Hanson, N. F. Hartmann, A. Singh, X. Ma, W. J. I. DeBenedetti, J. L. Casson, J. K. Grey, Y. J. Chabal, A. V. Malko, H. Htoon, J. A. Hollingsworth, *J. Am. Chem. Soc.* **2017**, *139*, 11081.